Journal of Materials Chemistry

Cite this: *J. Mater. Chem.*, 2012, **22**, 785

www.rsc.org/materials

FEATURE ARTICLE

Solution-processed organic nano- and micro-materials: design strategy, growth mechanism and applications

Ting Lei and Jian Pei*

Received 16th September 2011, Accepted 19th October 2011
DOI: 10.1039/c1jm14599a

Recently many efforts have been devoted to the investigation of organic nano- and micro-materials due to their unique properties and broad applications in organic field-effect transistors, organic light-emitting diodes, organic photovoltaics, photodetectors and superhydrophobic materials. In comparison with physical vapour deposition, solution processing provides a more convenient and cost-effective approach to obtain organic nano- and micro-materials with various morphologies, including wires, sheets and flowers. In this review, we use the basic concepts of supramolecular chemistry to discuss the molecular design strategy and growth mechanisms of various organic nano- and micro-structures, and their relationship with the corresponding applications.

Introduction

Organic nanomaterials, especially electronically active ones, have attracted increasing attentions in the last decade.[1–5] Inorganic materials, such as nanowires,[6,7] quantum dots[8] and carbon nanotubes,[9] are the major types of nanomaterials, if not exclusive. Compared to their inorganic counterparts, organic materials can provide advantages such as unlimited choices of building blocks, versatile modification of materials from the molecular level, high flexibility, low cost, and ease for large-area fabrication, which open up a bright vista for the next generation nanotechnologies and electronic devices.

The fabrication of organic nanomaterials relies mainly on two methods, physical vapour deposition (PVD) and solution processing. PVD is commonly carried out in a quartz tube by sublimating organic molecules at high temperature (250–450 °C), and then the organic vapour is cooled and crystallized in the low-temperature zone. This approach is usually used for organic molecules with low molecular weight and high thermostability,[10,11] which limits its scope for large molecules, oligomers and polymers. In contrast, without high temperature or complex facilities, solution processing is more convenient and can be used for large-area fabrication. At the same time, the growth conditions are easily adjusted by changing the solvents, temperature and even dopants to control the growth of organic

Beijing National Laboratory for Molecular Sciences (BNLMS), the Key Laboratory of Bioorganic Chemistry and Molecular Engineering of Ministry of Education, College of Chemistry and Molecular Engineering, Peking University, Beijing 100871, China. E-mail: jianpei@pku.edu.cn; Fax: (+86) 10-62751845; Tel: (+86) 10-62751845

Ting Lei

Ting Lei received his B.Sc. degree in chemistry from Peking University in 2008, while he was working in Prof. Pei's group. In the same year, he continued his study at the same group as a graduate student. His research includes: the synthesis and characterization of organic materials for polymer FETs and solar cells; the synthesis and mechanism investigation of organic nanol micro-materials.

Jian Pei

Prof. Jian Pei received his B.Sc. and Ph.D. degrees in organic chemistry from Peking University. In 1998, he joined the group of Professor A. J. Heeger to study organic semiconducting materials. Since then he has stayed in Peking University since 2001. His research interests relate to organic synthesis, supramolecular chemistry, organic semiconductors, and optoelectronic devices.

nanomaterials. Therefore, solution-processed organic nanomaterials become more and more popular.

In this contribution, we describe recent progress in growth, self-assembly and applications of solution-processed organic nanomaterials. We also discuss the design strategy, different growth mechanisms, and their device performances in organic field-effect transistors (OFETs), organic light-emitting diodes (OLEDs), organic photovoltaics (OPVs), photodetectors and superhydrophobic materials *etc.*

Molecular design strategy and synthesis

Organic nanomaterials are formed by the self-assembly of organic molecules through different kinds of intermolecular interactions. The development of supramolecular chemistry paves the way to craft the growth of organic nanomaterials.[12]

π–π Interactions

π–π Interaction is the most favourable supramolecular interaction in the design of organic nanomaterials, especially for optoelectronic applications, because it not only provides a strong and directional interaction to render molecules growing in a certain direction, but also forms carrier transporting pathways by the overlap of molecular orbitals.[13,14] Despite the fact that π–π interaction is popular in this field, the strength of the π–π interaction and the causes of the interaction vary largely. The strength of π–π interaction ranges from 0 to 50 kJ mol^{-1}, sometimes comparable with van der Waals interactions, and sometimes even surpassing moderate hydrogen bonding.[12,13] The design strategy of π–π interacted nanomaterials is originated from the design of discotic liquid crystal molecules.[15,16] Both the strong π–π interaction between aromatic cores and the relatively weak interaction of side alkyl chains make these molecules show strong one-dimensional (1D) growth tendency. Under certain circumstances, the growth of the other two dimensions is confined, which results in 1D micro/nanowires.[17] Construction of large aromatic cores is the central topic to design and synthesize novel materials used for 1D organic nanomaterials. Oxidative dehydrogenation reactions, developed by Müllen *et al.*, are very powerful to construct large fused aromatic cores (Scheme 1),[15] such as hexa-*peri*-hexabenzocoronene (HBC, **1**) and its derivatives.[14] Nuckolls *et al.* reported the synthesis of an HBC isomer **2**, because the strain in the periphery of the compound made the molecule bend significantly away from planarity, where iodo-oxidative photocyclization reaction was employed.[18] Several aromatic cores containing thiophene units have been realized in our lab.[19–21] The oxidative C–C bond formation between two β-positions of thiophene units produced the target molecule **3** in 83% yield.

Sulphur–sulphur interactions

Along with π–π interactions, several weak non-covalent interactions play important roles in organic crystals. C–H···π interactions widely exist in oligoacenes and polycyclic aromatic hydrocarbons, such as pentacene[22] and perylene.[2] However, computational study showed that this kind of interaction always hindered the carrier transport in organic crystal because it reduced the face-to-face overlaps of aromatic cores.[22] Sulphur–sulphur interactions behave as a very important driving force to shorten the intermolecular distance in crystals, which appear in several organic semiconductors.[23,24] Recently, we synthesized tetrathienoanthracene **4** to investigated its OFET performance.[21] Perepichka *et al.* also synthesized **4** and its isomer **5** to compare their crystal packing and device performance.[25] As indicated in Fig. 1a and b, there are several close S···S interactions existing in the crystals. They found that both solution-processed and vacuum-deposited films, isomer **5** showed higher hole mobility than **4**. Wang *et al.* reported the synthesis of perylo[1,12-*b*,*c*,*d*]thiophene **7** and dithioperylene **8**.[26,27] After incorporating sulphur atoms into the perylene core, S···S interactions drove these molecules to form ideal face-to-face packing in crystals. Compound **7** was used to fabricate single-crystalline micrometre wire-based FETs through physical vapour deposition. The transistor devices exhibited p-channel behaviour with a mobility of 0.8 $cm^2\ V^{-1}\ s^{-1}$.[26] High mobility up to 2.13 $cm^2\ V^{-1}\ s^{-1}$ was achieved from 1D single crystal nanoribbons fabricated with **8** by solution process.[27]

Donor–acceptor interactions

The weak interaction between electron-rich and electron-deficient aromatic units has been proven to be a unique driving force for the formation of supramolecular assemblies.[28,29] On the other hand, an electron donor and acceptor (EDA) interaction is beneficial for organic solar cells, as an interpenetrating network is required to achieve highly efficient charge separation.[30] Recently, a truxene derivative **9** with a C_3 symmetric conjugated plane and its oxidized counterpart, truxenone **10**, were used to construct 1D microwires (Fig. 2).[31] In this system, absorption

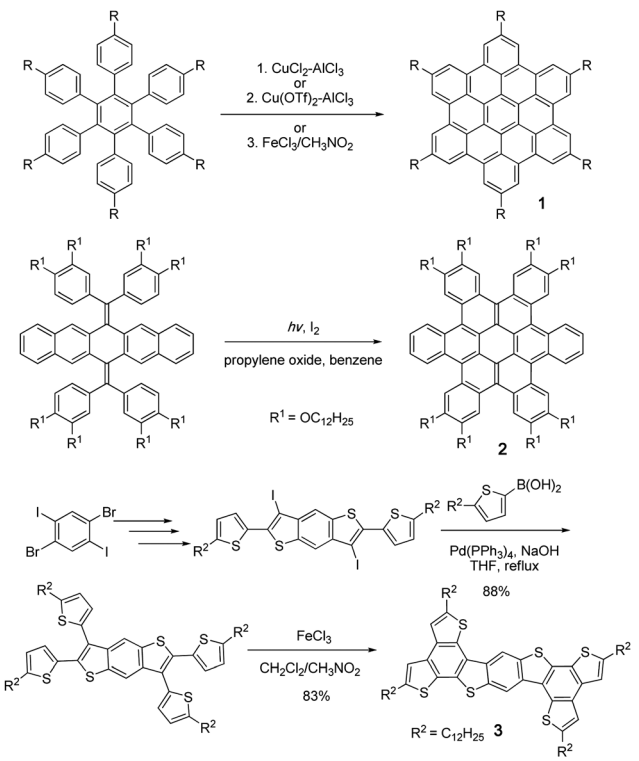

Scheme 1 Oxidative cyclization to construct large fused aromatic molecules.

spectra, ^{1}H NMR, differential scanning calorimetry (DSC), polarized optimal microscopy (POM) and X-ray diffraction (XRD) were employed to explore their donor–acceptor interaction. A Job plot demonstrated a 1 : 1 stoichiometry, as expected for EDA interactions. Furthermore, DSC, POM and XRD showed that a novel phase formed after their 1 : 1 mixing. The perfect match in structure, size, and symmetry of **9** and **10** provided an ideal platform for investigating the co-assembly between electron-rich and electron-deficient molecules.

Hydrophobic interactions

Although the strength of the hydrophobic interaction is hard to evaluate, it is extremely important for life processes, such as the formation of membranes, micelles and protein folding. Experimental data show that the stabilization of the compact state of a protein is, attributed to hydrophobic interactions, originating from van der Waals interactions among the aggregated non-polar groups in the protein and the strong entropic compensation when water molecules in the surfaces of every separated non-polar group are distributed back into the bulk solvent after the aggregation.[32] Using hydrophobic interactions to stabilize supramolecular structures has frequently been reported, and is well summarized by Lee and Stupp *et al.*[33,34] A typical example using hydrophobic interactions to built organic nanomaterials was reported by Aida *et al.* They synthesized HBC derivatives containing both hydrophobic alkyl and hydrophilic tetraethylene glycol (TEG) chains (Fig. 3). These molecules self-assembled into well-defined 1D bilayer tubular structures.[35–37] The structures were mainly stabilized by the π–π interactions from the HBC cores, van der Waals interactions of the alkyl chains and hydrophobic interactions. The alkyl chains were buried in the bilayer wall to avoid contacting with the hydrophilic environment.

Very recently, we reported a two-dimensional bilayered nanosheet constructed from a butterfly-shaped molecule (Fig. 4).[38] This molecule also possessed both hydrophobic alkyl chains and hydrophilic TEG chains. It formed free-standing films in solution, which could be easily transferred to a substrate for

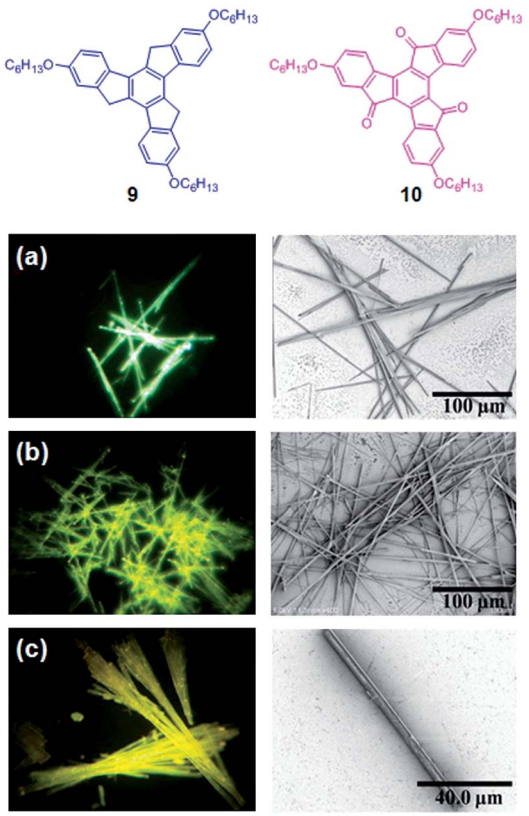

Fig. 2 The structures of **9** and **10** and fluorescence microscopy images (left, 400 magnitude), and scanning electron microscopy (SEM) images (right) of microwires of (a) **9**, (b) **10**, and (c) their 1 : 1 mixture precipitated from *n*-hexane (1 mg mL^{-1}).

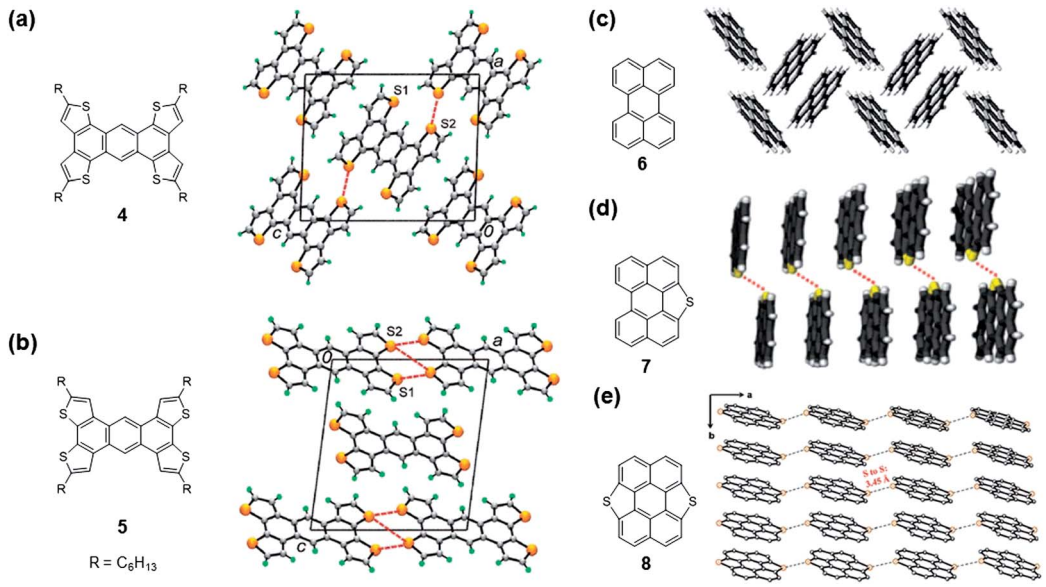

Fig. 1 Molecular structures and crystal packing of (a) tetrathienoanthracene **4**, (b) **4**'s isomer **5** (ref. 25); (c) perylene **6** (ref. 2*a*); (d) perylo[1,12-*b*,*c*,*d*] thiophene **7** (ref. 26) and (e) dithioperylene **8** (ref. 27). Sulphur–sulphur interactions drive the molecules to form ideal face-to-face packing in crystals. Reprinted with permission from ref. 2*a*, 25–27. Copyright 2007, 2008, 2010 and 2011 American Chemical Society.

direct device fabrication. XRD of the multilayer nanosheets gave well defined diffraction patterns that were attributed to the reflections from (001) to (005) planes, suggesting a typical lamellar structure. Selected-area electron diffraction (SAED) showed the π–π stacking interaction of the nanosheets parallel to the surface of the film. Atom force microscopy (AFM) height analysis showed such individual thin films with a uniform height of approximately 4.0 nm. Therefore, we concluded that the bilayer sheet was formed through strong π–π stacking, assisted by van der Waals interactions of long aliphatic chains. Since the exteriors of the bilayer sheets were surrounded by TEG chains, further aggregation was inhibited.

Hydrogen-bonding interactions

Nanowires based on π–π interactions have been intensively explored. However, because of serious self-quenching in π–π interacting systems, it is a great challenge to obtain highly fluorescent nanowires through self-assembly. Different from other non-covalent interactions, hydrogen bonding is directional and relatively strong.[39,40] Normal hydrogen bonds typically range in strength from *ca.* 4 to 60 kJ mol^{-1}, which is one order of magnitude larger than van der Waals forces (<5 kJ mol^{-1}).[12] Geometrical matching and directionality of hydrogen bonding provides an alternative method to form 1D nanowires with various properties. Recently, we reported a supramolecular polymer constructed by multiple hydrogen bonds, which formed uniform nanowires and possessed high solid-state fluorescent quantum efficiency (Φ_F: 22%) (Fig. 5).[41] The monomers containing a shape-persistent three-dimensional (3D) skeleton and hydrogen bonds were introduced in the vertical direction. The introduction of multiple hydrogen bonds not only provided a strong tendency of self-assembly in the vertical direction, but also lowered the possibility of the mismatch of hydrogen bonds. Moreover, the rigid 3D structure effectively reduced the self-quenching and aggregation to achieve high fluorescence efficiency in solid state. Interestingly, we also obtained single molecular nanowires with a width of only one single molecule from highly diluted solution because the horizontal van der Waals interaction was relatively weak (Fig. 5c).

Controlled growth and growth mechanism of organic nanomaterials

In order to obtain organic nanomaterials in expected sizes, shapes and morphologies, controlling both the self-assembly and the crystallization processes are very important. Several methods

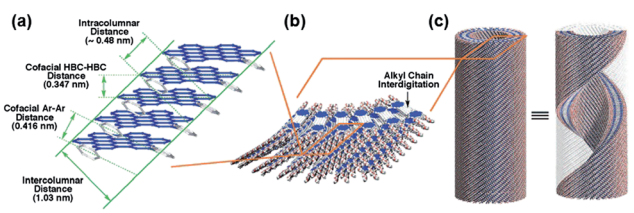

Fig. 3 Schematic representations of the hierarchical self-assembled structures of HBC derivatives reported by Aida *et al.* (a) π-stacked columnar array, (b) bilayer wall, and (c) nanotube. Reprinted with permission from ref. 37. Copyright 2008 American Chemical Society.

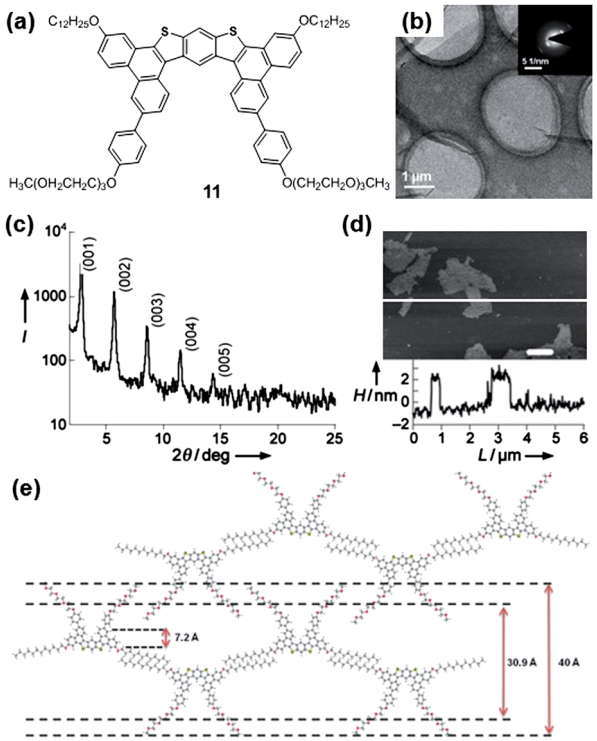

Fig. 4 (a) Molecular structure of the butterfly-shaped molecule. (b) Transmission electron microscopy (TEM), (c) XRD, and (d) AFM height images of the nanosheet. (e) Proposed model of the organization of the bilayer structure.

to control the growth of organic molecules into 1D nanomaterials have been proposed by Zang and Moore *et al.* recently, including rapid solution dispersion, phase transfer, vapour diffusion, seeded growth and sol–gel processing.[4] Although solution-processed organic nanomaterials can be modulated by several factors and many interesting morphologies have been reported, the growth mechanisms of organic nanomaterials and impact factors remain obscure. Simply, the growth of organic nanomaterials is always explained with traditional crystallographic knowledge—the confined growth of organic crystals. However, in-depth understanding of the growth mechanism and the molecular structure–morphology relationship requires inspirations from other domains and perspectives.

Alkyl chain effect and π–π stacking

Recently, Zang *et al.* reported the effect of side-chain substituents on the morphology of self-assembled perylene diimide molecules.[42] Two molecules, *N*,*N*′-di(nonyldecyl)-perylene-3,4,9,10-tetracarboxylic diimide **13** and *N*,*N*′-di(dodecyl)-perylene-3,4,9,10-tetracarboxylic diimide **14**, were synthesized to investigate their self-assembly behaviours (Fig. 6). These molecules exhibited different self-assembly behaviours in solution. Compared to **13** with branched alkyl chains, the emission from the aggregates of **14** was red-shifted significantly (about 30 nm), and its fluorescent quantum yield decreased by about three times. Moreover, the aggregates of **14** showed a pronounced absorption band at longer wavelength. These observations indicated a stronger intermolecular π–π stacking in the aggregates of **14**,

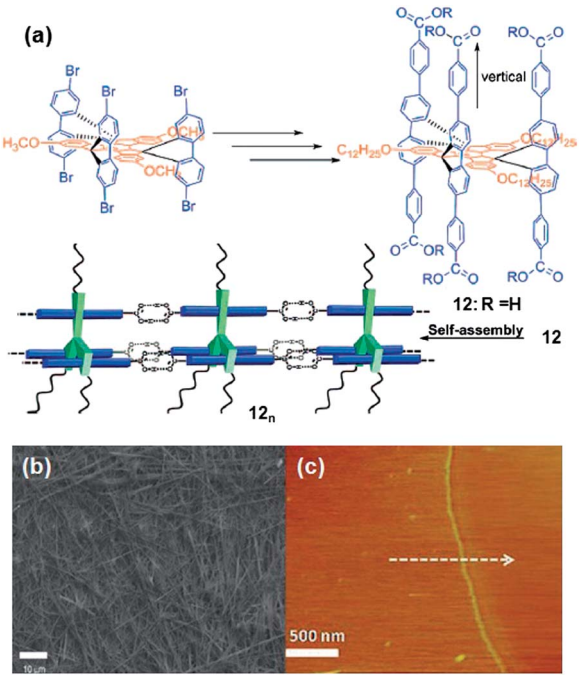

Fig. 5 (a) The structure of hexaacid **12** and the schematic diagram of its assembly **12n**. (b) SEM image of the nanowires formed from **12**. (c) AFM height image of single molecular nanowires formed from diluted solution.

which ultimately led to distinct outcomes of self-assembly: while **13** formed zero-dimensional nanoparticles, **14** formed 1D nanobelts (Fig. 6).

Isomeric effect and solvent effect

Competition between solute–solute interactions and solute–solvent interactions determines the equilibration of crystallization and dissolution, which control the growth of organic nanomaterials. Increasing the solute–solute interactions enhances the self-assembly of molecules, while increasing the solute–solvent interactions destroys the aggregates. Moreover, the solute–solute and solute–solvent interactions are determined by the molecular structure of the solute. Therefore, revealing the two mutually competitive interactions from the molecular level is critical for controlling the morphology of organic nanomaterials.

In order to understand the solute–solute and solute–solvent interactions, we synthesized three similar molecules (**17a**, **17b**, and **17c** as shown in Scheme 2) to investigate their self-assembly behaviours. These molecules have an identical truxenone core and different peripheries, which were obtained through a facile approach.[43]

Interestingly, the constitutional isomers, **17a** and **17b**, exhibited surprisingly large differences in solubility and DSC behaviours, suggesting different aggregation pathways. **17b** could readily dissolve in $CHCl_3$, while it is difficult to find a solvent to perform ^1H NMR titration experiments with the poor solubility of **17a**. DSC features of **17a** showed a melting point (T_m) at around 179 °C before decomposition (T_d); compound **17b**, on the other hand, exhibited a distinct glass transition temperature (T_g) at around 95 °C and a melting transition (T_m) at 128 °C. With more substituents, **17c** had better solubility as expected, and no T_g and T_m above 50 °C were observed before its T_d.

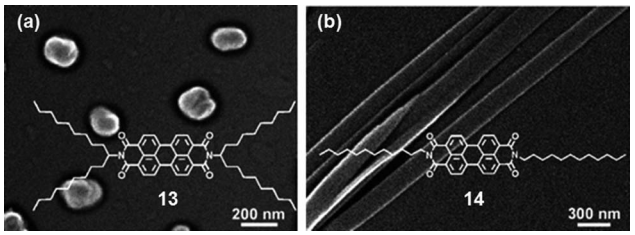

Fig. 6 Molecular structures and the self-assembly results (SEM images) of (a) **13** and (b) **14**. Reprinted with permission from ref. 42. Copyright 2006 American Chemical Society.

The SEM images showed the 1D microstructures of **17a**, **17b**, and **17c** in THF, dioxane, and *n*-hexane (Fig. 7), respectively. The responses of **17a–c** to these solvents differ greatly as a function of the solvent polarity. After heating their THF solution at a concentration of 1 mg mL^{-1}, then cooling down to room temperature, only **17a** formed 1D microbelts; **17b** and **17c** did not show any 1D structures under the same conditions. Upon changing to the moderately polar solvent dioxane, microbelts of **17a** with a similar width and length distribution to those observed with THF were obtained. In addition, uniform microbelts of **17b** clearly emerged, and microfibers of several hundreds of micrometres in length were readily formed from **17c**. Upon further decreasing the solvent polarity to *n*-hexane, no assembly structure of **17a** was observed due to its poor solubility. In contrast, microbelts of **17b** not only grew longer but also tended to be more rigid and straight, and irregular structures for **17c** were again observed in *n*-hexane.

The extensive calculations on their molecular properties demonstrated that for **17c**, the steric repulsion between the two adjacent side chains forced the alkoxy chains to flip out of the molecular plane in the equilibrium geometry. As a result, **17c** has a dipole moment of 1.99 D, whereas **17a** and **17b** are nonpolar due to their C_{3h} symmetry and nearly planar structures. This significant difference increased the solubility of **17c** in polar

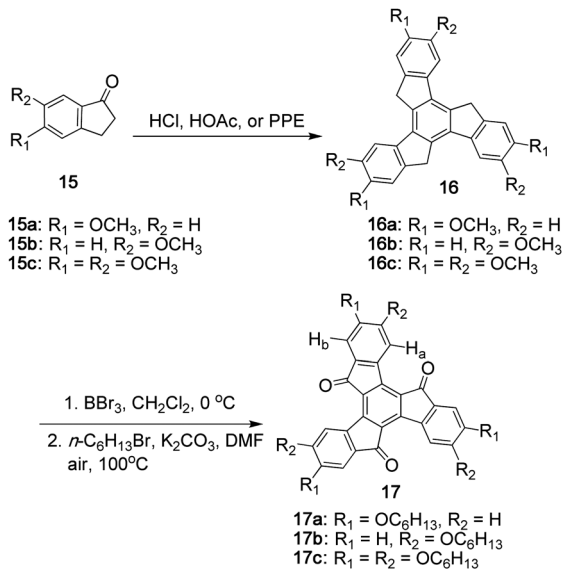

Scheme 2 Synthetic approach to three truxenone derivatives **17a–c**.

solvents such as THF. Moreover, the additional three hexyloxy chains increased van der Waals interaction between **17c** and *n*-hexane molecules, which hampered the growth of the 1D structure of **17c** in hexane.

For **17a** and **17b**, we found that the traceless quadruple moment of **17a** was about 50% larger than that of **17b**, suggesting a much stronger electrostatic interaction in stacked complexes of **17a**. To break such a strong intermolecular interaction in **17a**, a polar solvent such as THF should be employed to provide sufficient solubility for initiating the 1D self-assembly process. In the case of **17b**, with much weaker intermolecular interaction between the aromatic cores, instead of considering the solubility issue, less interference from solvent molecules became the key to obtain 1D assembly of **17b** successfully.

Organic microtwist and temperature effect

Chiral structures represent a fascinating type of architecture in nature, such as nanoscale DNA double-helix and macroscale chiral biominerals.[44] The twisted organic nanomaterials were usually observed in gel networks.[34,45] We reported an interesting example of well-separated microtwists from achiral X-shaped π-conjugated molecules *via* solution processing (Fig. 8).[46] Microwires of **18a** were obtained through dissolving the molecules in a mixture of $CHCl_3$ and EtOH (2 : 3 v/v) at a concentration of 1 mg mL^{-1} and then evaporating the solvents slowly (Fig. 8b). Surprisingly, by accelerating the precipitation rate of **18a**, *i.e.* cooling the hot homogeneous solution quickly to room temperature, multilevel branched structures with chiral twist were obtained. For **18b**, with longer alkyl chains, it self-assembled into a perfect twisted structure with uniform pitch. More importantly, branching was almost completely suppressed. Meanwhile, equal numbers of *P* and *M* twisted structures were obtained because there was no asymmetric factor present either in the molecules or in the environment.

We also observed that by simply adjusting the growth temperature for the microstructure, control over the pitch of the microtwist was easily achieved. Fig. 8c–e shows SEM images of the twists obtained at various temperatures. The general trend is that the slower the precipitation process, the larger the pitch. We speculated that the formation of the microtwist was due to its special crystal growth kinetics. We built a simple kinetic model and compared it with the experimental results, which were found to be in good accordance with each other. Therefore, we concluded that the imbalance of the growth rate between the centre and the edge provided the driving force for twisting.

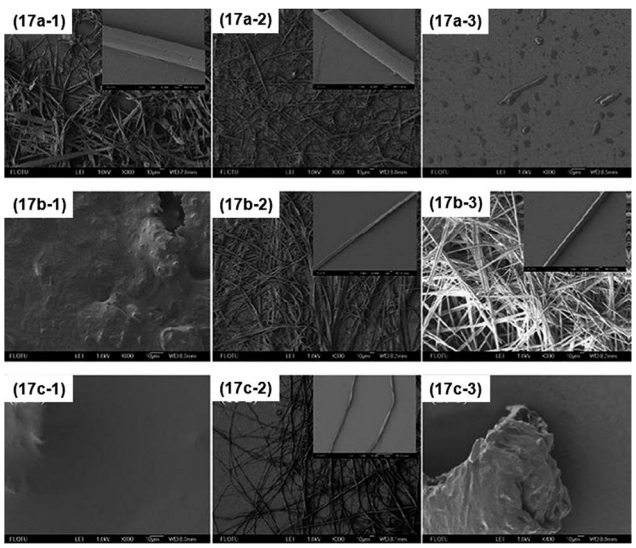

Fig. 7 SEM images of **17a–c** microstructures formed from 1: THF; 2: dioxane; 3: *n*-hexane. Scale bars: 10 μm.

Organic nano/micro-tube formed by etching

Nanotubular structures are very attractive due to their broad applications such as nano-transporters, nano-reaction containers, and high surface-area sensors.[40] Zhang and Lee *et al.* reported a single crystal micro-tube with a rectangular cross section formed by a molecule **19**.[47] **19** is a typical intramolecular-charge-transfer compound, and the intermolecular D–A interaction is the main driving force to direction the growth of the microtube (Fig. 9). The preparation is simple, and no surfactant, template, or catalyst was employed. Based on the observation of time-dependent growth, they proposed that the tubular structures were formed by etching or dissolving the center of a solid rectangular nanorod by THF. Because a high density of defects, which formed at the initial stage of crystallization, probably existed at the center of the rectangular nanorods, after the nanorods were formed, a higher etching or dissolution rate at

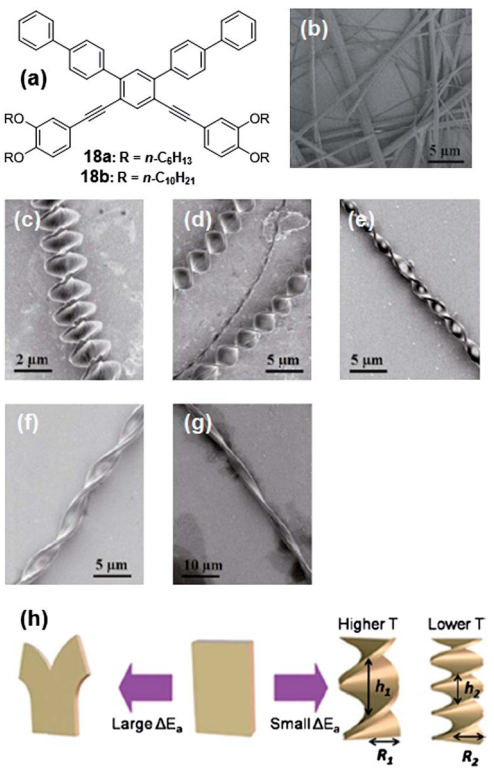

Fig. 8 (a) Structures of X-shaped molecules **18a** and **18b**. (b) SEM image of microfibers prepared from **18a**. SEM images of samples precipitated at (c) 15, (d) 20, (e) 25, (f) 30, and (g) 35 °C. (h) Schematic representation of the formation of bifurcated microstructure and twisted ribbons under different conditions.

the center than that of the exterior layer led to the formation of the hollow nanotubes.

Organic flowers formed by hierarchical self-assembly

Besides 1D ones, 2D and 3D nanostructures are also attractive. Several organic nanostructures, such as nanosheets[36] and nano/micro-flowers[48–51] have been reported. Nakanishi *et al.* reported a flower-shaped morphology based on hierarchically organized supramolecular nano-to-micro-architecture, readily prepared by self-organization of fullerene derivative **20** (Fig. 10).[48] The flower-like structures displayed well-defined diffraction peaks from (001) to (006) planes with a *d*-spacing value of 4.12 nm, consistent with high resolution (HR) cryo-TEM analysis at the flake edge of a flower-shaped object. The black dot in Fig. 10c marks the peak originating from the packing distance of neighbouring C_{60} moieties ($d = 0.91$ nm), which indicated a significant C_{60}/C_{60} π–π interaction. Therefore, the authors proposed that the flowers were formed through π–π interaction of C_{60} and van der Waals interaction of the interdigitated aliphatic chains. Very interestingly, after tracking the growth process of the flowers, Nakanishi *et al.* observed that disk-like assemblies were also formed. The rolling distortions took place in every quarter of the disk, resulting in square-shaped objects having four corners with conical shapes. When the rolling-up proceeded continuously, spatial congestions occurred at the four corners, resulting in crumpling, bending, stretching, and fracture of the disks. After completing these transformations, the bilayer growth at the edges continued, fixing the spatial conformation of the crumpled sheets (Fig. 10e). The nano/micro-flowers were formed by hierarchical assembly, which firstly formed disk-like multilayer structures, and then the disks continued to roll-up into a flower.

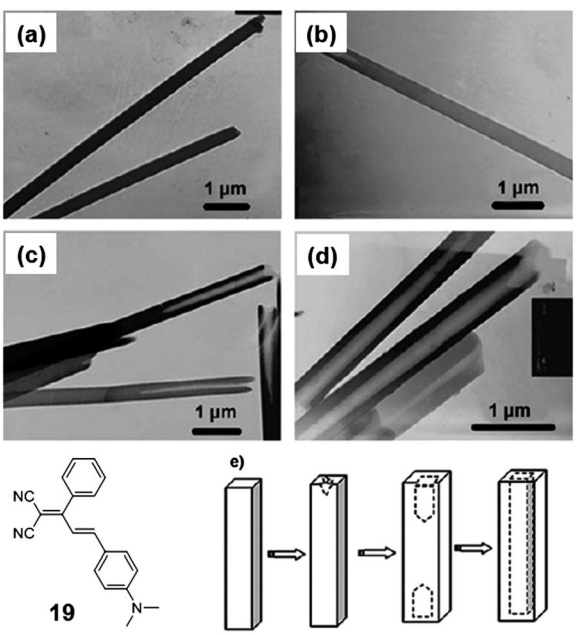

Fig. 9 TEM images of **19** samples obtained after stirring for a) 1 min, b) 10 min, c) 30 min, d) 4 h, and e) proposed process of tube formation. Reproduced with permission from ref. 47. Copyright 2007 Wiley-VCH Verlag GmbH & Co. KGaA.

A similar formation mechanism of flower-shaped supramolecular assemblies was also observed in the process of slowly cooling down a hot homogeneous solution of **21** and **22** to various temperatures.[48] As shown in Fig. 11a–f, only platelike and elliptical precursors were observed at the initial stage for **21**. We note that such flat objects consisted of stacked layers instead of a single layer. The edges of such precursors started to bifurcate in every direction (Fig. 11a, b, and c), and then to roll up to minimize the total elastic energy.[52] When the rolling-up behaviours proceeded continuously, the inner layers had more space to consequently bifurcate (Fig. 11d and e), resulting in a 3D flower-shaped object. Tracing the growth mechanism of flower-shaped assemblies formed by **22** gave a similar result (Fig. 11g–l). The formation mechanism indicates that the formation of the microscopic flower-like assemblies was determined by both spatial and energy factors. Moreover, we also found that slow aging was essential for the formation of flower-shaped assemblies.

Applications of organic nanomaterials

Reduction in size often does more than simply make things smaller. Many properties of materials, such as mechanical and optoelectronic properties, will change below a certain size scale.[51] Size dependent properties in inorganic nanomaterials are widely and systematically investigated.[6–9,53] However, their counterparts, organic nanomaterials, are seldom investigated. Recently, organic nanomaterials have exhibited very interesting properties and applications, which cannot be realized in bulky systems.

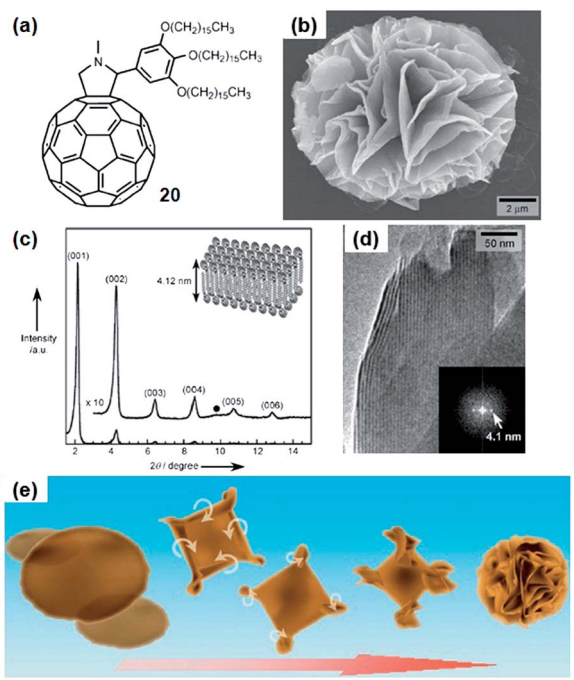

Fig. 10 (a) Molecular structure of fullerene derivative **20**. (b) SEM, (c) XRD and (d) HR-cryo-TEM image of the flower precipitated from 1,4-dioxane solution. (e) Schematic representation of the formation mechanism of the flower-shaped supramolecular assembly. Reproduced with permission from ref. 48. Copyright 2007 Wiley-VCH Verlag GmbH & Co. KGaA.

Moreover, these nanostructures are mostly obtained from simple solution processes, which are practical for low-cost and large-area fabrications.

Organic field-effect transistors

OFETs are of great importance for fabricating circuits, displays, and radio-frequency identification devices.[2,54] Generally, OFETs are fabricated into a polycrystalline film by PVD and solution processing. However, the mobility of the film is limited by defects such as inevitable grain boundaries. On the other hand, even details of the fabrication procedure, such as evaporation speed, substrate temperature and surface treatment, dramatically affect the final device performance. Therefore, it is hard to evaluate the intrinsic performance of organic molecules. Single crystal OFETs (SC-OFETs), ideally with long-range order and no defects, exhibited promising applications for evaluating the limitation of a specific material and understanding the mechanism of carrier transport in devices. At the same time, mobilities of SC-OFETs are usually better than their polycrystalline counterparts. But it is in general more difficult to obtain single crystals of organic molecules, and their fragility and brittleness prevented their large-scale fabrication, especially flexible device fabrication.

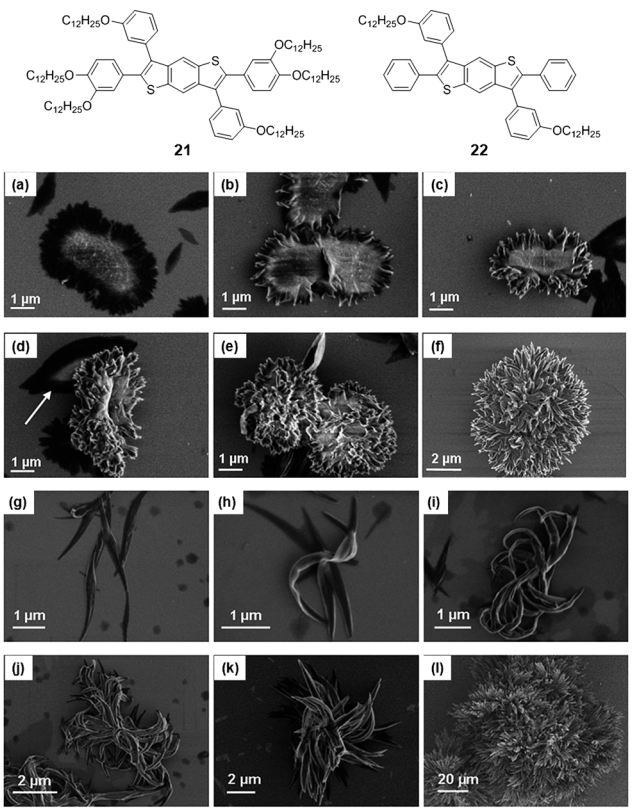

Fig. 11 SEM images of intermediates of flower-shaped supramolecular assemblies of (a–f) **21** and (g–l) **22**. For **21**, slowly cooling a hot homogeneous solution of **21** in $CHCl_3$/EtOH from 60 °C to (a) 50 °C, (b) 45 °C, (c) 40 °C, (d) 35 °C (the arrow shows the possible precursor for the flower formation), (e) 30 °C and (f) 25 °C. For **22**, when slowly cooling a hot homogeneous solution of **22** in $CHCl_3$/EtOH from 60 °C to (a and b) 50 °C, (c and d) 40 °C, (e) 35 °C and (f) 25 °C.

1D organic nanostructure provides another opportunity to achieve high mobility *via* easy processing. The 1D nanostructures are similar to single crystals with little grain boundaries, meanwhile they can be easily obtained either by PVD[55,56] or solution processing. Fig. 12 shows several recently developed organic nanostructures used for OFETs through solution processing. Hexathiapentacene (HTP, **23**) containing a pentacene core and hexa-sulphur periphery, was firstly reported for the fabrication of vacuum deposited thin film OFETs.[57] It gave a hole mobility of 0.04 $cm^2\ V^{-1}\ s^{-1}$. Bao *et al.* obtained single-crystal nanowires using HTP through solution processing (Fig. 12a).[58] SAED showed that the nanowires were growing along the 100 direction, which the π–π stacking pointed towards. The hole mobilites of single nanowires could be as high as 0.27 $cm^2\ V^{-1}\ s^{-1}$ with current on/off ratios $>10^3$. The previously discussed dithioperylene **8** nanowires fabricated by Wang and Pei *et al.* also showed high mobility up to 2.13 $cm^2\ V^{-1}\ s^{-1}$.[27] The nano/microwires of our molecule **3** were firstly obtained from CH_2Cl_2 solution, which showed a poor mobility of 0.01 $cm^2\ V^{-1}\ s^{-1}$.[17] However, by enhancing the crystallinity and crystal surface through a slow crystallization process in a mixture of THF/hexane, optimizing the interface between the dielectric layer, reducing the channel length through an improved plastic fiber mask method, and realizing asymmetric metal electrodes for source and drain, a hole mobility up to 2.1 $cm^2\ V^{-1}\ s^{-1}$ was obtained using the same molecule.[59] Triisopropylsilylethynyl pentacene (**TIPS-PEN**, **25**) is a popular pentacene derivative used for solution-processed thin film transistor fabrication.[60] The thin film OFETs fabricated with TIPS-PEN through solution processing reached a high mobility up to 1.8 $cm^2\ V^{-1}\ s^{-1}$ with an on/off ratio up to $\sim 10^8$.[61] Cho *et al.* reported the single-crystalline microribbons of **TIPS-PEN** preparation using the solvent-exchange method. The microribbons exhibited excellent performance showing a high mobility of 1.42 $cm^2\ V^{-1}\ s^{-1}$ and an on/off ratio of 10^5 (Fig. 12e).[62] Recently, we described the synthesis of a series of aceno[2,1,3]thiadiazole derivatives (**26**, Fig. 12f).[63] These molecules exhibited a column-like crystal packing, which were different from other **TIPS-PEN** derivatives. Although these molecules were designed for ambipolar transport, only hole-transporting was observed. The highest mobility of the nanowires fabricated with **26** was 0.4 $cm^2\ V^{-1}\ s^{-1}$. n-Type semiconducting nanowires are seldom reported due to the deficiency of air-stable n-type molecules. Bao *et al.* reported n-type nanowires fabricated with perylenetetracarboxyldiimide (**PTCDI**, **24**) (Fig. 12d).[64] The highest mobility measured for **24** was 0.027 $cm^2\ V^{-1}\ s^{-1}$. Complementary inverters based on n-channel **PTCDI** nanowire transistors and p-channel **HTP** nanowire OFETs were also fabricated and a gain as high as 8 was achieved. All the above nanowires have a common feature that the long axis of their crystal is along the π–π stacking direction. This result suggests that the π–π interactions are the main driving force to form such anisotropic crystals, and fortunately it is helpful for carrier transport because the π–π stacking direction is always a higher carrier transporting direction in SC-FETs.

Small molecules are not the exclusive ingredients for nanowire cuisine. Hu *et al.* reported well-defined, highly crystalline nanowires of a rigid rod conjugated polymer, a poly(*para*-phenylene ethynylene) derivative with thioacetate end groups (**TA-PPE**, **27**).[65] The TA-PPE nanowires were obtained by slow self-assembly from a solution under a certain solvent pressure in

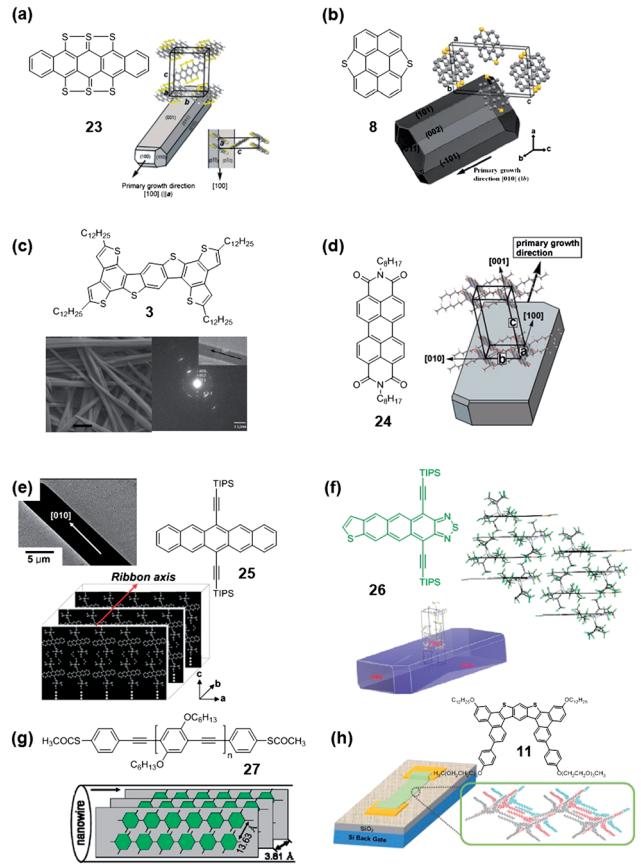

Fig. 12 Several recently developed organic nanostructures used for OFETs and their molecular packings. Nano/microwires fabricated with (a) HTP reported by Bao *et al.* in 2007 (ref. 58); (b) dithioperylene reported by Wang *et al.* in 2011 (ref. 27); (c) benzodithiophene derivative reported by Pei *et al.* in 2007 and 2010 (ref. 19 and 59); (d) PTCDI derivative reported by Bao *et al.* in 2007 (ref. 64); (e) TIPS-PEN reported by Cho *et al.* in 2007 (ref. 62); (f) aceno[2,1,3]thiadiazole derivative reported by Pei *et al.* in 2011 (ref. 63); (g) polymer **TA-PPE** reported by Hu *et al.* (ref. 65); (h) 2D nanosheet fabricated with a butterfly-shaped molecules reported by Pei *et al.* in 2011 (ref. 38). Reproduced with permission from ref. 27, 58, 64, and 65. Copyright 2007, 2009 and 2011 American Chemical Society. Reproduced with permission from ref. 62. Copyright 2007 Wiley-VCH Verlag GmbH & Co. KGaA.

a closed jar. The nanowires were highly crystalline with an orthorhombic crystal unit. OFETs based on these nanowires exhibited charge carrier mobility as high as 0.1 $cm^2\ V^{-1}\ s^{-1}$, 3–4 orders of magnitude higher than that of thin film transistors of the same polymer. Interestingly, the π–π stacking direction of the nanowires was predominantly perpendicular to the long axis of the nanowires (Fig. 12g), which was different from those small molecules discussed above. Compared with 1D ones, 2D organic nanomaterials for optoelectronics are seldom reported. Recently, we obtained a novel 2D nanosheet, and structure analysis showed that the π–π stacking interaction of the nanosheet was parallel to the surface of the sheet. Organic transistors with the highest mobility of 0.02 $cm^2\ V^{-1}\ s^{-1}$ have been successfully achieved (Fig. 12h).[38]

In order to deposit and align nanowires precisely in a desired position to fabricate large-scale integrated devices, Several bottom-up methods for inorganic materials have been exploited, such as vapor–liquid–solid (VLS) processes, the Langmuir–Blodgett (LB) assembly technique, electric-field-assisted alignment and dip coating.[7,66,67] However, simple and scalable patterning techniques to fabricate aligned arrays and devices for organic nanowires are rarely reported. Recently, we reported position- and size-controllable organic nanowire arrays made by a simple dip-coating method (Fig. 13).[68] Nanowire arrays with tunable length, desirable density and periodicity were realized by optimizing slip-stick motion, solvent evaporation conditions and the solution concentration. Parallel organic nanowires were directly grown and aligned on the substrate, and a hole mobility of $1 \times 10^{-4}\ cm^2\ V^{-1}\ s^{-1}$ was achieved. Bao *et al.* reported a filtration-and-transfer (FAT) alignment method. The FAT method enables facile control over both the alignment and density of MWs. They fabricated transistors composed of **BPE-PTCDI** mirowire networks by the FAT method.[69] Aligned microwires were transferred to the channel area of bottom contact substrates. The devices showed an average mobility of 0.24–0.07 $cm^2\ V^{-1}\ s^{-1}$ with current on/off ratios of 10^5 to 10^6.

Organic light-emitting diodes and organic photovoltaics

Although organic nanostructures are extensively investigated for OFETs, they are rarely directly used for fabrication of OLEDs and OPVs. We developed a novel approach to improve the performance of polymer OLEDs by blending a nanostructured dopant **28** as hole-transporting material into an electron-dominated **F8BT** polymer matrix (Fig. 14).[70] Because the organic nanowires of **28** self-assembled *in situ* within the device after spin-coating the mixture of **F8BT** and **28**, the fabrication of the nanoscale blended film is as simple as regular polymer blending. At a 2.5 wt% concentration of nanowires, the luminous efficiency of **F8BT** device increased from 4.29 to 8.25 cd A^{-1}, and external quantum efficiency increased from 1.0 to 1.92%. For pristine **F8BT** devices, the hole mobility was beyond the detectable limit. But for devices doped with 1, 2.5, and 5 wt% nanowires, the hole mobilities were 2×10^{-7}, 5×10^{-7}, and $1 \times 10^{-6}\ cm^2\ V^{-1}\ s^{-1}$, respectively. Apparently, the device performance was improved

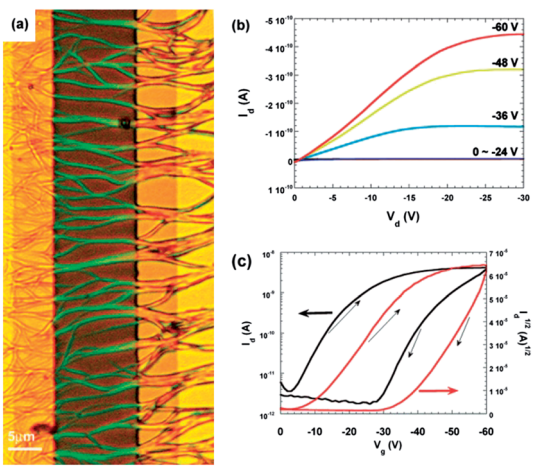

Fig. 13 (a) Optical image of the FET device based on the nanowire array. (b) Output characteristics of the FET. (c) Transfer characteristics of the FET.

as a result of increased hole mobility of the device by doping the nanowires.

To improve the power conversion efficiency (PCE) of solar cells, a good phase separation and high carrier mobilities are required.[71] Nuckolls *et al.* reported a new type of organic semiconductor device structure, in which organic nanostructures were used as the donor of the solar cells.[72] They synthesized a new molecule, dibenzotetrathienocoronene **29**, which self-assembled into columnar superstructures (Fig. 15b). The devices were fabricated by spin-coating **29** on PEDOT:PSS, followed by evaporation C_{60} to form a bilayered structure (Fig. 15e). The highest PCE of 1.9% was obtained for the devices annealed at 150 °C before C_{60} deposition. The authors found that after annealing, some nanostructures were formed (Fig. 15c and d). This was an interesting heat-induced self-assembly process, which led to a large effective interfacial area and interdigitated networks.

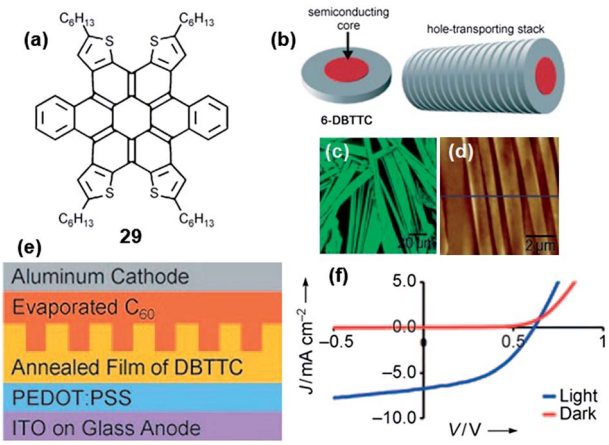

Fig. 15 (a) Molecular structure of **29**. (b) Illustration of the assembly of **29** into hole-transporting columns. (c) Fluorescence microscopy and (d) AFM images of films of **29** annealed at 150 °C. (e) The OPV device architecture with a nanostructured active layer. (d) Typical current density–voltage (J–V) curves for a **29** device. Reproduced with permission from ref. 72. Copyright 2010 Wiley-VCH Verlag GmbH & Co. KGaA.

Photodetectors

In our group, highly sensitive, air-stable photo-detectors based on organic crystalline nanowires of **3** were also fabricated.[73] The photoconductivity gain was about 1.3×10^3, while the responsivity was about 420 A W^{-1} at a field of 2×10^4 V cm^{-1}. The highest on/off ratio reached 1000. Fig. 16a showed the on/off switching properties of the detector using Au as electrode. The rise time of the photocurrent curve was short, while the falling time was long. The slow decay of the photocurrent after switching off the light suggested a typical trap releasing current. Compared with the devices using Au electrodes, devices fabricated with Al electrodes had a much lower photoconductivity gain and faster switching, we assumed that thermal evaporation of heavy metal Au onto the organic nanowires produced much more surface states than the evaporation of Al. Therefore, the long lifetime of the trapped photogenerated carriers in the surface states gave rise to the high photo gain and the slow photocurrent decay of the Au-electrode device.

Photowaveguides

1D organic nanomaterials for active waveguide with high efficiency are required to process good fluorescent emission, proper crystal dimensions, and smooth crystal surfaces.[5] However, for conventional 1D organic nanomaterials formed by π–π stacking, the fluorescent quantum efficiencies are quite low because of strong intermolecular electronic interactions. In order to enhance emission in solid state, we attempted to enlarge the intermolecular distance of adjacent aromatic rings by introducing steric hindrance. Five molecules were designed based on pyrazino[2,3-*g*]quinoxaline (**PyQ**) units following this principle (Scheme 3).[74]

We systematically analysed the photophysical properties of these five molecules, which showed typical D–A characteristics. The crystal structures were also resolved to understand the molecular packing in these molecules. The microfibers formed by molecules **30** and **31** exhibited relatively low self-quenching, together with desirable crystal dimensions and surfaces. They were proved to be low-loss waveguide materials (0.02–0.05 dB/μm), as shown in Fig. 17.

We also investigated the photowaveguide properties of the X-shaped molecules, which could form both microwires (Fig. 8a) and microtwists (Fig. 18).[75] The microwires showed excellent properties in low-loss long-distance (4.9 dB/100 μm, >200 μm) photowaveguide in a single wire. However, microtwists showed only a medium performance (8.3 dB/100 μm) because the microtwists were not well crystallized and the surfaces were imperfect. Usually, waveguiding materials have simple geometric shapes such as wires or ribbons. This is the first investigation of

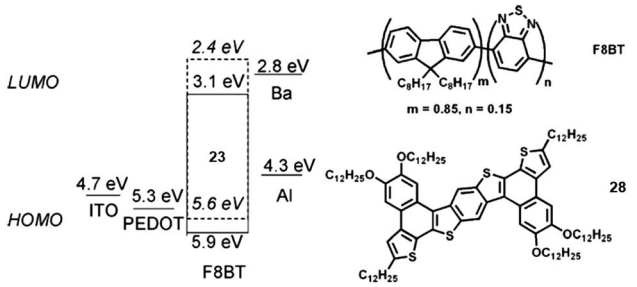

Fig. 14 Schematic depiction of the device configuration and the energy diagram and molecular structures of the materials used in the active layers.

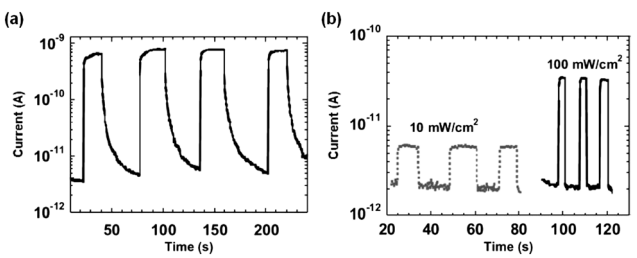

Fig. 16 The reproducible on/off switching properties of the photodetector exposed to the 405 nm laser at a bias of 20 V: (a) Au–Au device under 11 mW cm^{-2} irradiation. (b) Al–Al device under 10 mW cm^{-2} irradiation (dotted line), and 100 mW cm^{-2} irradiation (solid line).

waveguiding property for a chiral material. Interestingly, we also observed coupling effect between microwires (Fig. 18c and d), which indicated the potential of organic nanostructures in building complex optical system in micrometre or submicrometre scale.

Gas and explosives detection

Organic molecules have been widely explored as sensors used for gas sensing, explosives detection, and biological applications. Traditionally, organic molecules used for detection are stored in solution or fabricated into films.[76,77] However, solution is not suitable for practical applications such as portable devices; film is good for practical usage but it always has a small surface area, which limits its detection scope. Organic nanostructures with high surface areas provide another choice. We reported that by simply drop casting the solution of **3** in different solvents, three different well-controllable organic nanostructures, including 1D microbelts and 3D flower-shaped nanostructures (type A and type B), were facilely self-assembled (Fig. 19).[78] In the application of those structures to detect explosives, with the evolution of structures from netted 1D microbelts to flower-shaped nanostructures, the detection speed of the chemosensors for 2,4-dinitrotoluene (DNT) and 2,4,6-trinitrotoluene (TNT) was improved by more than 700 times. Our investigation revealed that the morphology control is crucial for detection due to largely different surface areas.

Superhydrophobic materials

Most organic materials are intrinsically hydrophobic. However, in order to realize superhydrophobic materials, the fractal morphology of the two-tier roughness on both micro- and nanometre scales is required.[79,80] Nakanishi *et al.* used their fullerene derivatives to self-assemble into globular objects of macroscopic dimensions with a wrinkled, flake-like sub-micrometre structure at the outer surface. The films formed by globular objects possessed high thermal stability and durability towards various polar solvents, with a water contact angle of 152.0°.[47]

We reported two kinds of microscale flower-shaped morphologies with nanometre petals formed from the hierarchical self-assembly of **21** and **22**.[50] As shown in Fig. 20, two kinds of flowers exhibited distinct morphologies. The films formed by two morphologies showed excellent water-repelling characteristics as superhydrophobic surfaces. One film displayed a superhydrophobic surface (contact angle > 161°) with little sliding angles (<3°); another film presented an adhesive superhydrophobic surface, and the water droplets were pinned on the surface even when it was turned upside down. Interestingly, the transition process from the Cassie state to the Wenzel state was easily realized by slightly changing the chemical structures.

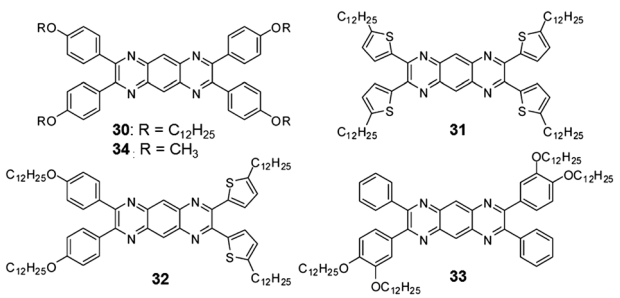

Scheme 3 Five molecular structures based on **PyQ**.

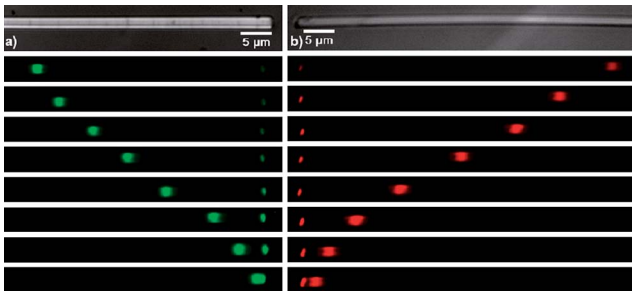

Fig. 17 Waveguide characterizations of the microfibers of **30** and **31**. Fluorescent microscope photographs of the microfibers of (a) **30** and (b) **31** (grey value images and painted with false colour).

Modification of nanowires

It is difficult to design a new molecule with expected morphology. Therefore, modifying a well-developed molecule for a special purpose becomes a common approach to extend its application. Aida *et al.* used this strategy to functionalize their amphiphilic HBC molecule to realize diverse functions such as photoconductivity.[36] However, this strategy is not general for other molecules, especially for π–π interacting systems because the introduced functional groups always interfere with the original π–π interactions, resulting in unexpected morphologies. Therefore, direct modification of the surface of nanomaterials is more convenient and versatile. In order to demonstrate this approach, we developed a facile method to modify the surface of a fragile organic 1D microstructure (Fig. 21).[81] The bulk molecules and surface modifiers were designed with orthogonal solubility to protect the molecular crystals from destruction under the reaction conditions. Because the microwires formed by **Blue-Br** (**34**)

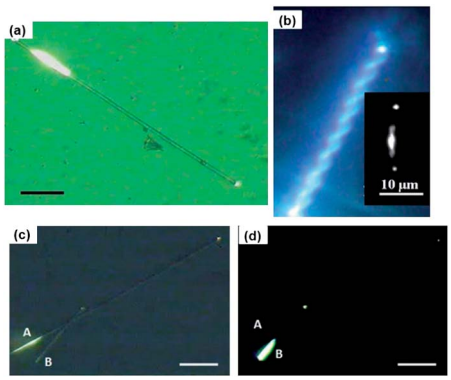

Fig. 18 Waveguide characterizations of the microfibers of **18a** and **18b**. Fluorescent microscope photographs of the microfibers of (a) **18a** and (b) **18b** (grey value images and painted with false colour). (c) Coupling effect in a two-ribbon system in bright field, excitation position: left end of microribbon A. (d) A corresponding picture of the two-ribbon system in dark field, excitation position: left end of microribbon B.

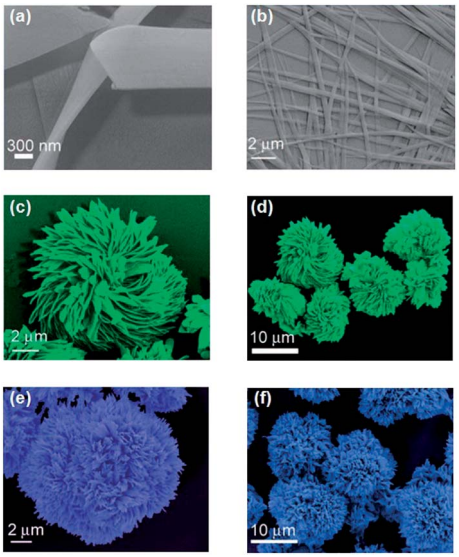

Fig. 19 SEM images of different crystalline nanostructures: (a and b) microbelt, (c and d) flower A, and (f and g) flower B self-assembled from 1,4-dioxane, THF, and n-decane solutions, respectively.

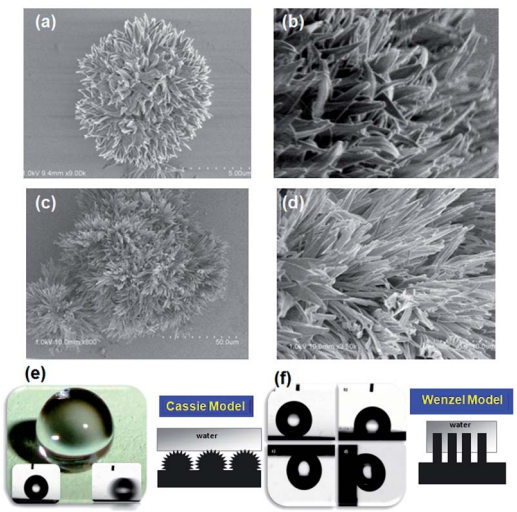

Fig. 20 SEM images of nanoflowers formed by (a and b) **21**, and (c and d) **22**. (e) Pictures of film formed by nanoflowers of **21** and the water droplet on the surface. The film was analysed with the Cassie model. (f) Water droplet on the surface of nanoflowers of **22**, which was analysed with the Wenzel model.

were insoluble in ethanol, while **Red-OH** was soluble, the reactions were performed in ethanol using K_2CO_3 as a base. After attempting various conditions (Fig. 21d), we proved that **Red-OH** was covalently bonded to the nanowires. The nanowires emitted white light with CIE coordinates of ($x = 0.32$, $y = 0.36$). Moreover, using fluorescent lifetime mapping (Fig. 21c), we found that the modification happened on the surface of the nanowires. Compared with other methods, our strategy not only needs a very small amount of the modifiers, but also well preserves the morphologies.

Another approach to surface modification of organic nanostructures is non-covalent modification. Although this modification is not stable in solution, it works well under dry conditions. After our covalent approach, Zang *et al.* reported an interfacial modification of the electron-deficient nanofibrils formed by perylene diimide **36** with electron-rich carbazole **37** (Fig. 22).[82] This surface modification formed a "surface heterojunction", and the nanofibril showed high photoconductivity with fast photoresponse. In this design, the alkyl chains not only guaranteed the absorption of the modifiers, but also spatially separated the photogenerated charge carriers to prevent their combination.

Summary and perspectives

The past couple of years have witnessed great growth in the development of organic nano- or micro-materials. The development of supramolecular chemistry provided fruitful principles to help us design molecules and control the growth of the materials by solution processes. Detailed investigation of the growth mechanisms of various types of nano/micro-materials also provided us with further insight into the design and control of the nano/micro-structures. However, we have to admit that our understanding towards design strategies and growth mechanisms is, sometimes, superficial, and controlling the growth still needs some fortune.

Compared with bulk organic materials, reduction in size really exhibited attractive and exciting properties: nano/micro-structures for OFETs combined the high performance of single crystals and the flexibility of thin films; nano/micro-structures increased the carrier mobility of OLEDs, and enhanced the charge separation of the OPVs; because of their high surface area, they also improved the detection limit of organic materials; organic materials are usually hydrophobic, but nanoflowers realized superhydrophobic properties. Reduction in size of organic materials indeed offered traditional organic materials

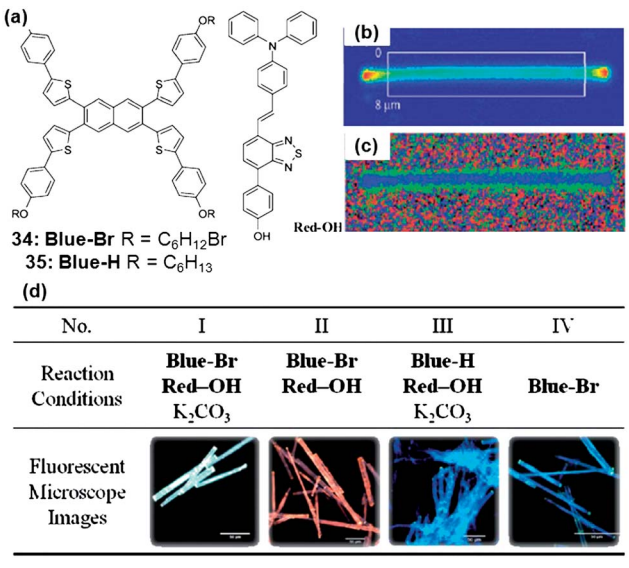

Fig. 21 (a) Molecular structures used in the study. (b) Intensity mapping of the WLE microwires. (c) Lifetime mapping of WLE microwires excited at 485 nm; blue colour indicated the region with a short lifetime. (d) Experimental results under different reaction conditions.

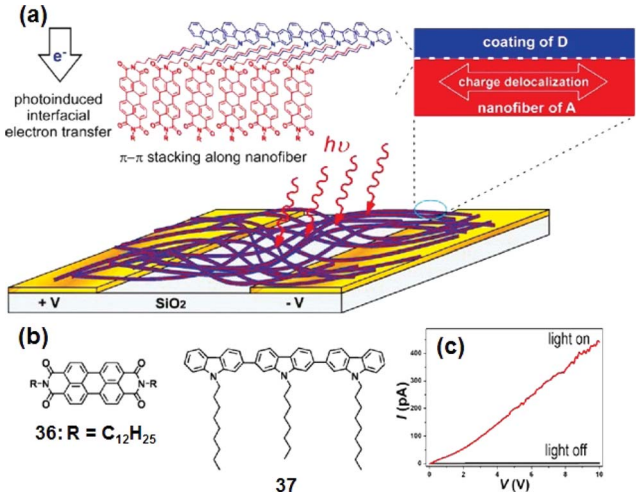

Fig. 22 (a) Schematic illustration of nanofibril heterojunctions developed by Zang *et al.* (b) Molecular structure used in the study. (c) *J–V* curves of the nanowires in response to turning on and off the white light irradiation. Reprinted with permission from ref. 82. Copyright 2011 American Chemical Society.

novel and unique properties, which show a bright future for further investigation of organic nano/micro-materials.

Acknowledgements

This work was financially supported by the Major State Basic Research Development Program (No. 2009CB623601) and by the National Natural Science Foundation of China (NSFC). We thank Prof. Xiao-Yu Cao (Xiamen University) for his suggestions and insightful discussion.

Notes and references

1 P. Pramod, K. G. Thomas and M. V. George, *Chem.–Asian J.*, 2009, **4**, 806.
2 (*a*) R. Li, W. Hu, Y. Liu and D. Zhu, *Acc. Chem. Res.*, 2010, **43**, 529; (*b*) L. Jiang, H. Dong and W. Hu, *J. Mater. Chem.*, 2010, **20**, 4994.
3 F. S. Kim, G. Ren and S. A. Jenekhe, *Chem. Mater.*, 2011, **23**, 682.
4 L. Zang, Y. Che and J. S. Moore, *Acc. Chem. Res.*, 2008, **41**, 1596.
5 Y. S. Zhao, H. Fu, A. Peng, Y. Ma, Q. Liao and J. Yao, *Acc. Chem. Res.*, 2010, **43**, 409.
6 J. Hu, T. W. Odom and C. M. Lieber, *Acc. Chem. Res.*, 1999, **32**, 435.
7 Y. Xia, P. Yang, Y. Sun, Y. Wu, B. Mayers, B. Gates, Y. Yin, F. Kim and H. Yan, *Adv. Mater.*, 2003, **15**, 353.
8 A. J. Nozik, M. C. Beard, J. M. Luther, M. Law, R. J. Ellingson and J. C. Johnson, *Chem. Rev.*, 2010, **110**, 6873.
9 P. J. F. Harris, *Carbon Nanotubes and Related Structures: New Materials for the Twenty-First Century*, Cambridge University Press, 1999.
10 Q. Tang, H. Li, Y. Liu and W. Hu, *J. Am. Chem. Soc.*, 2006, **128**, 14634.
11 Y. Zhang, H. Dong, Q. Tang, S. Ferdous, F. Liu, S. C. B. Mannsfeld, W. Hu and A. L. Briseno, *J. Am. Chem. Soc.*, 2010, **132**, 11580.
12 J. W. Steed and J. L. Atwood, *Supramolecular Chemistry* (2nd Edition.), John Wiley & Sons Ltd. Publication, 2009.
13 F. J. M. Hoeben, P. Jonkheijm, E. W. Meijer and A. P. H. J. Schenning, *Chem. Rev.*, 2005, **105**, 1491–1546.
14 V. Coropceanu, C. Jérôme, D. A. da Silva Filho, Y. Olivier, R. Silbey and J.-L. Brédas, *Chem. Rev.*, 2007, **107**, 926.
15 J. Wu, W. Pisula and K. Müllen, *Chem. Rev.*, 2007, **107**, 718.
16 S. Sergeyev, W. Pisula and Y. H. Geerts, *Chem. Soc. Rev.*, 2007, **36**, 1902.
17 M. Kastler, W. Pisula, D. Wasserfallen, T. Pakula and K. Müllen, *J. Am. Chem. Soc.*, 2005, **127**, 4286.
18 S. Xiao, J. Tang, T. Beetz, X. Guo, N. Tremblay, T. Siegrist, Y. Zhu, M. Steigerwald and C. Nuckolls, *J. Am. Chem. Soc.*, 2006, **128**, 10700.
19 Y. Zhou, W.-J. Liu, Y. Ma, H. Wang, L. Qi, Y. Cao, J. Wang and J. Pei, *J. Am. Chem. Soc.*, 2007, **129**, 12386.
20 W. Liu, Y. Zhou, Y. Ma, Y. Cao, J. Wang and J. Pei, *Org. Lett.*, 2007, **9**, 4187.
21 J.-Y. Wang, Y. Zhou, J. Yan, L. Ding, Y. Ma, Y. Cao, J. Wang and J. Pei, *Chem. Mater.*, 2009, **21**, 2595.
22 E. F. Valeev, V. Coropceanu, D. A. da Silva Filho, S. Salman and J.-L. Brédas, *J. Am. Chem. Soc.*, 2006, **128**, 9882.
23 M. Mas-Torrent, M. Durkut, P. Hadley, X. Ribas and C. Rovira, *J. Am. Chem. Soc.*, 2004, **126**, 984.
24 H. Ebata, T. Izawa, E. Miyazaki, K. Takimiya, M. Ikeda, H. Kuwabara and T. Yui, *J. Am. Chem. Soc.*, 2007, **129**, 15732.
25 J. L. Brusso, O. D. Hirst, A. Dadvand, S. Ganesan, F. Cicoira, C. M. Robertson, R. T. Oakley, F. Rosei and D. F. Perepichka, *Chem. Mater.*, 2008, **20**, 2484.
26 Y. Sun, L. Tan, S. Jiang, H. Qian, Z. Wang, D. Yan, C. Di, Y. Wang, W. Wu, G. Yu, S. Yan, C. Wang, W. Hu, Y. Liu and D. Zhu, *J. Am. Chem. Soc.*, 2007, **129**, 1882.
27 W. Jiang, Y. Zhou, H. Geng, S. Jiang, S. Yan, W. Hu, Z. Wang, Z. Shuai and J. Pei, *J. Am. Chem. Soc.*, 2011, **133**, 1.
28 C. Wang, S. Yin, S. Chen, H. Xu, Z. Wang and X. Zhang, *Angew. Chem., Int. Ed.*, 2008, **47**, 9049.
29 W. Zhang, W. R. Dichtel, A. Z. Stieg, D. Benítez, J. K. Gimzewski, J. R. Heath and J. F. Stoddart, *Proc. Natl. Acad. Sci. U. S. A.*, 2008, **105**, 6514.
30 T. M. Clarke and J. R. Durrant, *Chem. Rev.*, 2010, **110**, 6736.
31 J.-Y. Wang, J. Yan, L. Ding, Y. Ma and J. Pei, *Adv. Funct. Mater.*, 2009, **19**, 1746.
32 P. L. Privalov and S. J. Gill, *Adv. Protein Chem.*, 1988, **39**, 191.
33 H.-J. Kim, T. Kim and M. Lee, *Acc. Chem. Res.*, 2011, **44**, 72.
34 L. C. Palmer and S. I. Stupp, *Acc. Chem. Res.*, 2008, **41**, 1674.
35 J. P. Hill, W. Jin, A. Kosaka, T. Fukushima, H. Ichihara, T. Shimomura, K. Ito, T. Hashizume, N. Ishii and T. Aida, *Science*, 2004, **304**, 1481.
36 Y. Yamamoto, T. Fukushima, Y. Suna, N. Ishii, A. Saeki, S. Seki, S. Tagawa, M. Taniguchi, T. Kawai and T. Aida, *Science*, 2006, **314**, 1761.
37 W. Jin, Y. Yamamoto, T. Fukushima, N. Ishii, J. Kim, K. Kato, M. Takata and T. Aida, *J. Am. Chem. Soc.*, 2008, **130**, 9434.
38 J. Yin, Y. Zhou, T. Lei and J. Pei, *Angew. Chem., Int. Ed.*, 2011, **50**, 6320.
39 T. F. A. De Greef, M. M. J. Smulders, M. Wolffs, A. P. H. J. Schenning, R. P. Sijbesma and E. W. Meijer, *Chem. Rev.*, 2009, **109**, 5687.
40 D. T. Bong, T. D. Clark, J. R. Granja and M. R. Ghadiri, *Angew. Chem., Int. Ed.*, 2001, **40**, 988.
41 J. Luo, T. Lei, L. Wang, Y. Ma, Y. Cao, J. Wang and J. Pei, *J. Am. Chem. Soc.*, 2009, **131**, 2076.
42 K. Balakrishnan, A. Datar, T. Naddo, J. Huang, R. Oitker, M. Yen, J. Zhao and L. Zang, *J. Am. Chem. Soc.*, 2006, **128**, 7390.
43 J.-Y. Wang, J. Yan, Z. Li, J.-M. Han, Y. Ma, J. Bian and J. Pei, *Chem.–Eur. J.*, 2008, **14**, 7760.
44 D. L. Nelson and M. M. Cox, *Lehninger Principles of Biochemistry* (4th edition), W.H. Freeman and Company: New York, 2005.
45 V. K. Praveen, S. S. Babu, C. Vijayakumar, R. Varghese and A. Ajayaghosh, *Bull. Chem. Soc. Jpn.*, 2008, **81**, 1196.
46 H.-B. Chen, Y. Zhou, J. Yin, J. Yan, Y. Ma, L. Wang, Y. Cao, J. Wang and J. Pei, *Langmuir*, 2009, **25**, 5459.
47 X. Zhang, X. Zhang, W. Shi, X. Meng, C. Lee and S. Lee, *Angew. Chem., Int. Ed.*, 2007, **46**, 1525.
48 T. Nakanishi, K. Ariga, T. Michinobu, K. Yoshida, H. Takahashi, T. Teranishi, H. Möhwald and D. G. Kurth, *Small*, 2007, **3**, 2019.
49 T. Nakanishi, T. Michinobu, K. Yoshida, N. Shirahata, K. Ariga, H. Möhwald and D. G. Kurth, *Adv. Mater.*, 2008, **20**, 443.
50 J. Yin, J. Yan, M. He, Y. Song, X. Xu, K. Wu and J. Pei, *Chem. Eur. J.*, 2010, **16**, 7309.
51 L. Wang, Y. Zhou, J. Yan, J. Wang, J. Pei and Y. Cao, *Langmuir*, 2009, **25**, 1306.
52 T. Shimizu, M. Masuda and H. Minamikawa, *Chem. Rev.*, 2005, **105**, 1401.
53 G. Hodes, *Adv. Mater.*, 2007, **19**, 639.

54 C. Reese and Z. Bao, *Mater. Today*, 2007, **10**, 20.
55 Q. Tang, H. Li, M. He, W. Hu, C. Liu, K. Chen, C. Wang, Y. Liu and D. Zhu, *Adv. Mater.*, 2006, **18**, 65.
56 Q. Tang, H. Li, Y. Liu and W. Hu, *J. Am. Chem. Soc.*, 2006, **128**, 14634.
57 A. L. Briseno, Q. Miao, M.-M. Ling, C. Reese, H. Meng, Z. Bao and F. Wudl, *J. Am. Chem. Soc.*, 2006, **128**, 1557.
58 A. L. Briseno, S. C. B. Mannsfeld, X. Lu, Y. Xiong, S. A. Jenekhe, Z. Bao and Y. Xia, *Nano Lett.*, 2007, **7**, 668.
59 Y. Zhou, T. Lei, L. Wang, J. Pei, Y. Cao and J. Wang, *Adv. Mater.*, 2010, **22**, 1484.
60 J. E. Anthony, *Angew. Chem., Int. Ed.*, 2008, **47**, 452.
61 S. K. Parka, T. N. Jackson, J. E. Anthony and D. A. Mourey, *Appl. Phys. Lett.*, 2007, **91**, 063514.
62 D. H. Kim, D. Y. Lee, H. S. Lee, W. H. Lee, Y. H. Kim, J. I. Han and K. Cho, *Adv. Mater.*, 2007, **19**, 678.
63 T. Lei, Y. Zhou, C.-Y. Cheng, Y. Cao, Y. Peng, J. Bian and J. Pei, *Org. Lett.*, 2011, **13**, 2642.
64 A. L. Briseno, S. C. B. Mannsfeld, C. Reese, J. M. Hancock, Y. Xiong, S. A. Jenekhe, Z. Bao and Y. Xia, *Nano Lett.*, 2007, **7**, 2847.
65 H. Dong, S. Jiang, L. Jiang, Y. Liu, H. Li, W. Hu, E. Wang, S. Yan, Z. Wei, W. Xu and X. Gong, *J. Am. Chem. Soc.*, 2009, **131**, 17315.
66 N. Ranjan, H. Vinzelberg and M. Mertig, *Small*, 2006, **2**, 1490.
67 J. Huang, R. Fan, S. Connor and P. Yang, *Angew. Chem., Int. Ed.*, 2007, **46**, 2414.
68 N. Liu, Y. Zhou, L. Wang, J. Peng, J. Wang, J. Pei and Y. Cao, *Langmuir*, 2009, **25**, 665.
69 J. H. Oh, H. W. Lee, S. Mannsfeld, R. M. Stoltenberg, E. Jung, Y. W. Jin, J. M. Kim, J.-B. Yoo and Z. Bao, *Proc. Natl. Acad. Sci. USA*, 2009, **106**, 6065.
70 Q. Niu, Y. Zhou, L. Wang, J. Peng, J. Wang, J. Pei and Y. Cao, *Adv. Mater.*, 2008, **20**, 964.
71 G. Dennler, M. C. Scharber and C. J. Brabec, *Adv. Mater.*, 2009, **21**, 1323.
72 A. A. Gorodetsky, C.-Y. Chiu, T. Schiros, M. Palma, M. Cox, Z. Jia, W. Sattler, I. Kymissis, M. Steigerwald and C. Nuckolls, *Angew. Chem., Int. Ed.*, 2010, **49**, 7909.
73 Y. Zhou, L. Wang, J. Wang, J. Pei and Y. Cao, *Adv. Mater.*, 2008, **20**, 3745.
74 X. Wang, Y. Zhou, T. Lei, N. Hu, E.-Q. Chen and J. Pei, *Chem. Mater.*, 2010, **22**, 3735.
75 T. Lei, H.-B. Chen, J. Yin, S. Huang, X. Zhu and J. Pei, *Org. Electron.*, 2011, **12**, 453.
76 R. M. Crooks and A. J. Rico, *Acc. Chem. Res.*, 1998, **31**, 219.
77 S. W. Thomas III, G. D. Joly and T. M. Swager, *Chem. Rev.*, 2007, **107**, 1339.
78 L. Wang, Y. Zhou, J. Yan, J. Wang, J. Pei and Y. Cao, *Langmuir*, 2009, **25**, 1306.
79 X. Feng and L. Jiang, *Adv. Mater.*, 2006, **18**, 3063.
80 L. Jiang, X. Yao, H. Li, Y. Fu, L. Chen, Q. Meng, W. Hu and L. Jiang, *Adv. Mater.*, 2010, **22**, 376.
81 X. Wang, J. Yan, Y. Zhou and J. Pei, *J. Am. Chem. Soc.*, 2010, **132**, 15872.
82 Y. Che, H. Huang, M. Xu, C. Zhang, B. R. Bunes, X. Yang and L. Zang, *J. Am. Chem. Soc.*, 2011, **133**, 1087.

